26

Application of Forward Error Correcting Algorithms to Positioning Systems

Nikos Petrellis, Fotios Gioulekas, Michael Birbas,
John Kikidis and Alex Birbas
Analogies S.A., Patras Scientific Park
Greece

1. Introduction

The indoor localisation of a mobile target is an important issue in many robotics, automation, virtual reality and pervasive computing environments. The most sophisticated method for indoor localisation is based on processing the images captured by cameras that are placed on the target in order to recognise familiar landmarks and their distance (Jin et al, 2004); (Porta & Krose, 2006); (Clerentin et al, 2005); (Tovar et al, 2006); (Se et al, 2002). Image processing in conjunction with other localisation approaches described below (Borenstein et al., 1996) is very popular in autonomous robotics applications making feasible the familiarisation of a robot with unknown areas. Stochastic processing is often applied in this case in order to evaluate an estimated position. Nevertheless, expensive sensors and processing units are required in order to support the high computational complexity of this approach.

More popular lower cost approaches are based either on measuring the round trip time of a reflected wave or the strength of a signal. In the first case, the cost is higher if optical or laser scanning is employed since very short time intervals have to be measured with high precision (Miura et al, 2006); (Clerentin et al, 2005); (Victorino et al, 2003); (Arras et al, 2001). Ultrasonic signals can offer a lower cost alternative to this approach since the sonar waves travel with much lower speed than light but their main drawback is that this type of signal is not directional enough (Smith & Zografos, 2005); (Minami et al, 2004); (Tardos et al, 2002); (Bicho et al, 2000); (Baskent & Barshan, 1999). Moreover, it is more difficult to isolate the sonar transmitter from the receiver in order to reassure that only the reflected signal will be received.

Measuring the signal strength of multiple transmitters (Ladd et al, 2005); (Flora et al, 2005) can also provide an indication about the target position. This technique has already been adopted in cellular phone, Wireless Local Access Network (WLAN) or Bluetooth applications. Although wide areas can be covered in these networks, the distance estimation error is usually higher than half a meter. Even magnetic fields have been used for the accurate non-contact control of tools and medical instruments (Schlageter et al, 2001); (Kosel et al, 2005). The distance measured in this approach cannot be longer than some tenths of centimetres although a distance estimation of up to 10m has been reported in (Prigge & How, 2004).

Source: Pattern Recognition Techniques, Technology and Applications, Book edited by: Peng-Yeng Yin,
ISBN 978-953-7619-24-4, pp. 626, November 2008, I-Tech, Vienna, Austria

Infrared light has been employed using either passive or active sensors in order to avoid obstacles, estimate distance (Jin et al, 2004); (Bicho, 2000) or to profile the surface of an object by recognising its texture (Aytac & Barshan, 2004); (Benet et al, 2002); (Novotny & Ferrier, 1999).
A low cost infrared–based solution that relies on recognising digital patterns has been presented in (Petrellis et al, 2007a and 2007b). The reception quality of the patterns that are sent by at least two transmitters that are placed around the covered area is utilised for estimating the position of the receiver. A calibration procedure, that is carried out once, before real time operation, familiarises the target with the area. During this stage, the target visits predetermined positions and enumerates the recognised patterns in a period of time. Using several types of patterns, a position identity can be formed by the success rate of each pattern type. During real time operation, the current position identity is compared to the identities that were estimated during the calibration stage and the closer position is selected. Specific regression techniques can be employed in order to reach a more accurate estimation of the real target position.
The speed and accuracy of the position estimation method described above are strongly affected by instant noise that has not been taken into account during the calibration stage. The estimation speed can be improved by increasing the frequency of the carrier that is used for the pattern transmission. In this way, shorter patterns can be employed. Several rules can be applied to validate the results of the position estimation procedure and discard false results caused by instant noise. In this case, the estimation procedure should be repeated for the specific position (Petrellis et al, 2007b).
In the present work, we employ Forward Error Correction (FEC) techniques in order to reduce the effect of instant noise and speed up the estimation procedure. The interleaving process employed in Turbo decoding can minimize the effect of the burst errors caused by the instant noise (Schlegel & Perez, 2004); (Kschischang et al, 2001); (Hagenauer et al, 1996); (Gamal & Hammons, 2001) (Arzel et al, 2007). Instead of recognizing a large number of long patterns as the case was in our previous work, a small number of short signatures are used. These signatures are encoded in both interleaved and uninterleaved form at the side of the transmitter and the resulting bit stream is broadcast as an infrared signal. When the attenuated signal is received at the target, it is corrected by a decoder that can be implemented either in software or by dedicated hardware (Gioulekas et al, 2005); (Bickerstaff et al, 2003). Since our localisation approach is based on the quality of the received signal, the intension is to minimise the burst errors caused by instant noise through the selected FEC method rather than fully correct all the errors.
The control of the error rate margins can be based on the study of the behaviour of the specific infrared channel and its noise sources. Choosing "equalised" signatures can minimise some types of errors. The new sampling method employed at the side of the receiver increases significantly the estimation speed. The processing overhead of the error correction is small compared to the duration of the infrared signatures used. Besides the speed enhancement, the accuracy and the estimation reliability is also improved.
The architecture of the infrared transmitters and receivers of the present work as well as their topology is described in Section 2. The infrared channel features are studied and the decoding algorithms used are discussed in Section 3 and Section 4 respectively. The simulation results are presented in Section 5. The different experimental pattern structures that were tested are described in Section 6. Finally, the experimental results are presented in Section 7 along with some discussion on the advantages and the disadvantages of the various pattern structures.

2. System architecture and topology

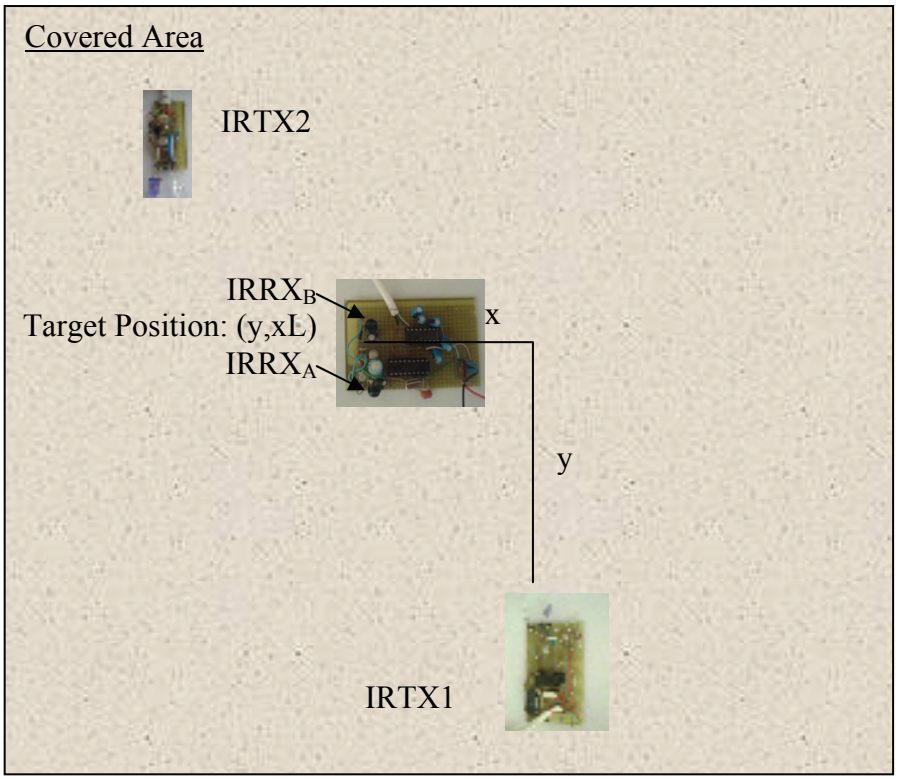

Fig. 1. The topology of the infrared transmitters and receivers

The Position Estimation System described in this work consists of 2 or more infrared transmitters (IRTX) positioned at the borders of the covered area as shown in Fig. 1. Each one of these transmitters is broadcasting a specific set of pattern types. The second IRTX device is basically used to break the symmetry between the right and the left side of the first IRTX device as well as to extend the covered area. Two infrared sensors are placed at the target facing opposite directions. The main transmitting device (IRTX1) is used as a reference for the position of the target. The coordinates of the target in Fig. 1, are (y,xL), meaning that the target has horizontal and vertical distance x and y respectively and is positioned at the left (L) side of the IRTX1.

The architecture of an infrared transmitter is shown in Fig. 2. The processing unit of the IRTX device is responsible for the generation of the supported infrared patterns. It is also responsible for the encoding and the interleaving of the transmitted information although the encoded and interleaved form of the original signatures may have been stored a priori in the memory of the IRTX device. The patterns are transmitted over a carrier that may also be generated by the processing unit of the transmitter in order to reduce external circuitry. The patterns and the carrier are mixed and amplified before the infrared emitting diode is driven. More than one infrared emitting diode may be connected in parallel and placed in

circular arrangement in order to cover a wider area. In the present setup we used two diodes in parallel in both IRTX devices.
Different IRTX devices should be wired if they share the same processing unit. Independent IRTX devices may also be employed but this may have an impact on the estimation speed, accuracy and cost as will be discussed in Sections 6 and 7.

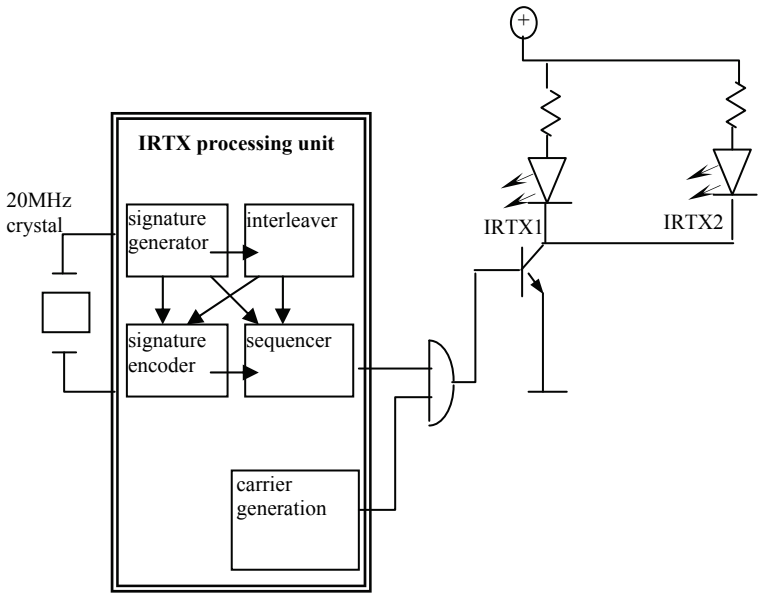

Fig. 2. Architecture of the IRTX device

The architecture of the receivers (IRRX devices) that are mounted on the target is presented in Fig. 3. An IRRX device accepts only the signals that were modulated on a specific carrier frequency. This is achieved through a bandpass filter and a carrier rejection circuitry that may be embedded in the infrared sensor if a standard carrier frequency is used. The use of the carrier protects from the interference of other infrared sources like the sunlight. The processing unit of the receiver is responsible for the sampling of the input signal and the recognition of the limits of the signatures, the encoded parity bits, etc. The received interleaved or uninterleaved signatures along with the parity bits are input to the Decoder and the Interleaver blocks. The corrected patterns are sent to a host computer that estimates the position of the target. The results of the position estimation could be utilised by other applications installed on the host computer. The decoding and error correction of the received signatures can be alternative performed by the host computer instead of the processing unit of the receiver. This is mandatory for a decoding algorithm that is based on complicated high precision arithmetic operations that cannot be handled by a low cost microcontroller.
The patterns transmitted by the IRTX devices in (Petrellis et al, 2007) are described in Fig. 4. The transmission starts with a preamble that is actually a long pause period. Then, a constant number of identical patterns are sent. These patterns are of the same type and each one consists of *i* pulses. These patterns are named MOD*i* and are separated by a pause

interval. Then, another set of MOD*j* patterns is transmitted with different number of pulses (*j*). In the example of Fig. 4, the preamble is followed by two MOD2 and one MOD4 pattern. The pulse width is not the same for different patterns types. More specifically, the pulse width in MOD*i* is chosen to be longer than the pulse width of MOD*j*, if $i<j$. In this way, MOD*i* patterns can be recognised with lower error rate than MOD*j* patterns. The number of MOD*i* patterns that are recognised at the receiver is the success rate of MOD*i*. The set of the success rates of all the supported pattern types forms an identity for a specific position. The receiver simply counts rising or falling edges between the pause intervals of the input signal, in order to recognise a pattern. Although the sampling is a simple procedure in this case, the pause intervals between the patterns lead to higher convergence times and lower estimation speed.

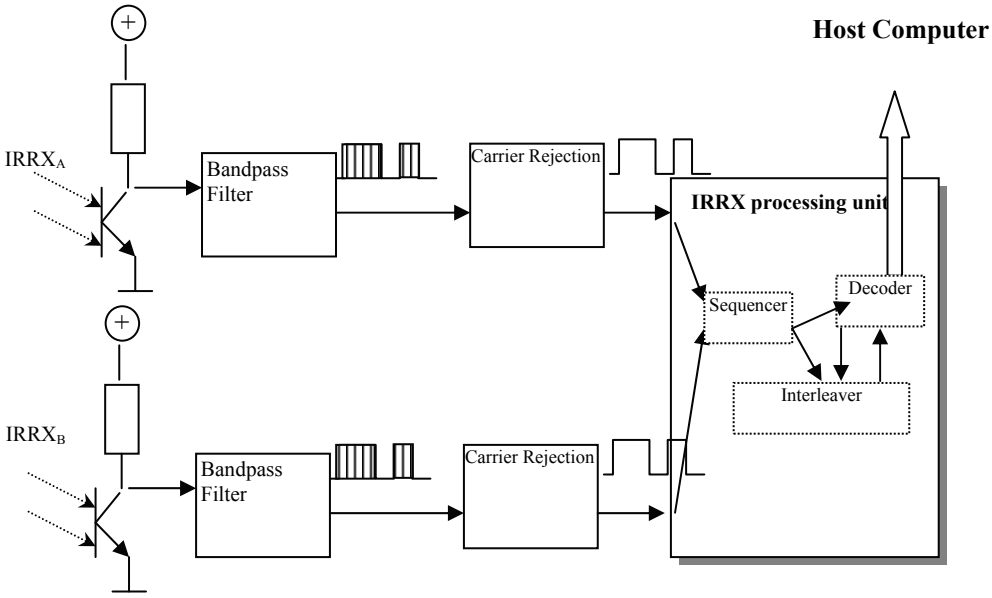

Fig. 3. Architecture of the IRRX devices

The sampling method described above cannot be applied if the transmitted patterns are not just a sequence of identical pulses. If more complicated signatures are transmitted, the receiver should sample the input signal at regular time intervals.

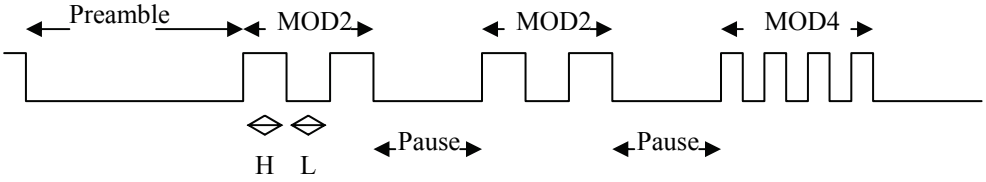

Fig. 4. The patterns transmitted in (Petrellis et al, 2007)

Consider for example the case where the signature 0x01 followed by the parity bytes 0x01 and 0x68 have to be transmitted as shown in Fig. 5a. The preamble in this case is again a long pause interval followed by a Start File Delimiter (SFD). As an SFD we selected the binary code 101. In general, the preamble is followed by the SFD, the original signature (SGN1), the parity bits of SGN1 (PA1) and the parity bits of the interleaved SGN1 (PB1) as shown in Fig. 5b. The code rate of this transmission is 1/3 if the PA1 and PB1 are considered as redundant information. Alternatively, the interleaved SGN1 can also be transmitted in order to increase the error correcting capability of the receiver (code rate 1/4).

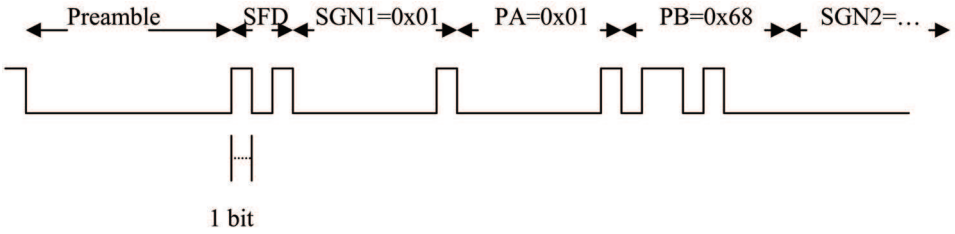

(a)

Preamble	SFD	SGN1	PA1	PB1	SGN2	PA2	PB2	SGN3

(b)

Fig. 5. Signature transmission in the present work

All the transmitted bits have the same width that is known to the receiver. The receiver has the option to sample the input signal sometime within the bit transmission period. If this single sampling occurs at a noisy time period the bit will not be recognised correctly. For this reason, we choose a different sampling scheme: if the bit period is T_b the input signal is sampled S_b times at regular time intervals of T_b/S_b. If more than $S_b/2$ of the samples are found to be logic '1', the specific bit is recognised as logic '1', otherwise as '0'. This procedure is shown in Fig. 6. Using the scheme described in Fig. 5 and Fig. 6, no pause intervals are necessary between the signatures and the parity info and hence, the position estimation speed is significantly improved.

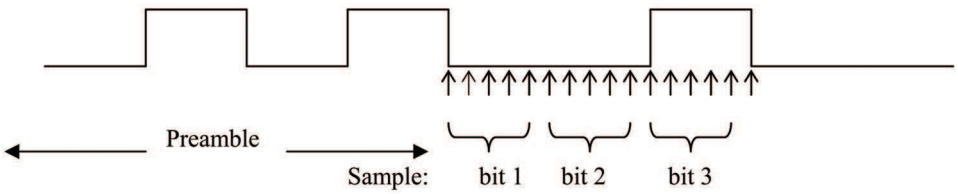

Fig. 6. Bit recognition based on the majority of samples

The retrieved signatures and parity bits are input to the interleaver and the decoder at the side of the receiver. These two modules are attempting to correct some error bits. Nevertheless, this is not always feasible due to the low Signal to Noise Ratio of the channel. The receiver may accept or ignore the results of the error correcting method since it is aware of the expected signature and parity bits. The matching degree of the received signatures with the expected ones forms an identity of the corresponding position.

Before the real time operation of the system, the target visits predetermined position in the covered area (e.g., the nodes of a virtual grid) and stores the matching degree of the various patterns that were retrieved at each node. During real time operation, the matching degrees estimated at the current target position are compared to the stored ones and the closer node is selected. The real target position can be further approximated if a two dimensional interpolation search is applied (Petrellis et al, 2007a).

3. Error sources in the specific infrared channel

The estimation of the distortion posed by the infrared channel in the transmitted signal is very important since the selection of the appropriate patterns and correction method can modify the bit error rate features of the reception. The experimental study of the errors that appear in the various patterns shows that we can distinguish five error sources: (a) reflections, (b) sampling method (c) scrambling of patterns transmitted by different IRTX devices, (d) signal attenuation and (e) random errors.

As already mentioned in the previous section, during the transmission of a logic '1', the IRTX device sends a high pulse modulated at the carrier frequency while nothing is sent during the transmission of a logic '0'. The infrared light transmitted when a '1' is sent reaches directly the receiver but is also reflected at the walls and the obstacles of the environment. Although the reflected infrared light fades soon, it is possible that the receiver will interpret a '10' transmission as a '11' since some additional samples can still be interpreted as '1' during the transmission of the second bit. Hence, the channel has memory due to the Inter-Symbol Interference (ISI) caused by the reflections since the currently received bit value depends on the previously transmitted one. If the environment favours reflections, the previous 2 bits that were transmitted may still affect the value of the current bit but their contribution is different in that case. By adopting the model used in the Partial Response channels of the magnetic storage media (Vasic & Kurtas, 2005), the reflections and the random errors of a channel are expressed as:

$$y(t) = \sum_{k=0}^{M_c} a_k x(t-k) + n(t) \tag{1}$$

$$\sum_{k=0}^{M_c} a_k^2 = 1 \tag{2}$$

$$\sigma^2 = N_0/2, \quad SNR = \frac{E_b}{2\sigma^2} = \frac{E_C}{2R\sigma^2} \tag{3}$$

$$A(D) \equiv \sum_{k=0}^{M_c} a_k D^k \tag{4}$$

The parameter x(t) is the transmitted bit while y(t) is the received one at the time point t. M_c is the memory of the channel i.e., the number of previous bits that affect the current one. The parameter n(t) expresses the Additive White Gaussian Noise (AWGN) of the channel with variance σ^2 (where E_c is the energy per coded bit, E_b is the energy per uncoded bit and $N_0/2$ is the (two-sided) noise power spectral density . If expression (2) is valid, then the Signal to

Noise Ratio (SNR) of the channel is estimated by (3). Fig. 7 shows the ISI of the current bit with the previous two bits.

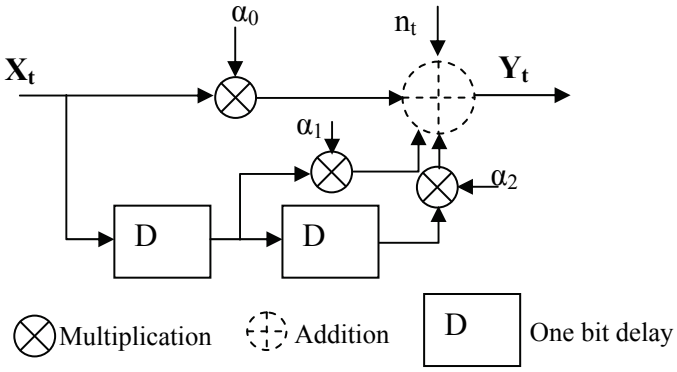

Fig. 7. Description of 2-bit interference scheme in the specific infrared channel

The sampling method described in the previous paragraph determines the value of the current bit from the majority of the samples retrieved in a period of time equal to the duration of the bit transmission. This method may lead to false recognition of a bit for two reasons: (a) the majority of the samples are noisy or (b) lack of synchronisation. The synchronisation is carried out when a preamble is sent. The lack of synchronisation may occur if a long bit sequence is transmitted and will usually affect the last bits of this sequence. It usually appears in the received pattern as an early recognised logic '1'. For example, the transmission of '01' may be recognised as '11' at the receiver.

The patterns transmitted concurrently by different IRTX devices are received by the two IRRX devices mounted on the target either directly or through reflections. For example, if IRTX1 is facing $IRRX_A$ and IRTX2 is facing $IRRX_B$, then if both IRTX devices transmit a logic '1', this bit will be probably recognised correctly by the two IRRX devices. Nevertheless, if the IRTX devices do not transmit the same bit value, both the IRRX devices may recognise a logic '1' due to the reflected signal of the IRTX device that transmits a logic '1'.

The signal of an IRTX device is attenuated if the target is positioned at a long distance from the transmitter. This is the main noise source that is responsible for the recognition of a transmitted logic '1' as a logic '0'. The errors caused by signal attenuation are considered to have been generated by a Rayleigh-like effect and expression (1) becomes:

$$y(t) = a_R(t) \sum_{k=0}^{M_c} a_k x(t-k) + n(t) \tag{5}$$

$$\Pr(a_R(t)) = 2l(t)e^{-l(t)^2}\ ,\ a_R(t)>0 \tag{6}$$

Equation (6) represents the probability density function for the Rayleigh parameter $a_R(t)$, while l(t) is the distance of the receiver from the transmitter.

All the noise sources described above can be combined in the pair of expressions that describe how each IRRX device is expected to receive the signals transmitted by the two IRTX devices:

$$y_A(t) = a_R(t) \sum_{k=-1}^{M_c} a_k x_1(t-k) + a_R(t) \sum_{k=-1}^{M_c} a_k' x_2(t-k) + n(t) \quad (7)$$

$$y_B(t) = a_R(t) \sum_{k=-1}^{M_c} a_k x_2(t-k) + a_R(t) \sum_{k=-1}^{M_c} a_k' x_1(t-k) + n(t) \quad (8)$$

The IRTX1 and IRTX2 devices transmit the input signals $x_1(t)$ and $x_2(t)$ respectively while $IRRX_A$ receives $y_A(t)$ and $IRRX_B$ receives $y_B(t)$. The summation starts from k=-1 in order to include the sampling errors. The parameter M_c is practically less or equal than 2. The second summation term at the right side of both (7) and (8) represents the reflected signal that is transmitted by the IRTX device that is not facing the specific IRRX sensor. Since the reflected signal is more attenuated compared to the signal that is received directly, it holds that:

$$a_k \geq a_k', \forall k \quad (9)$$

Some of the error types described above are shown in the example of Fig. 8.

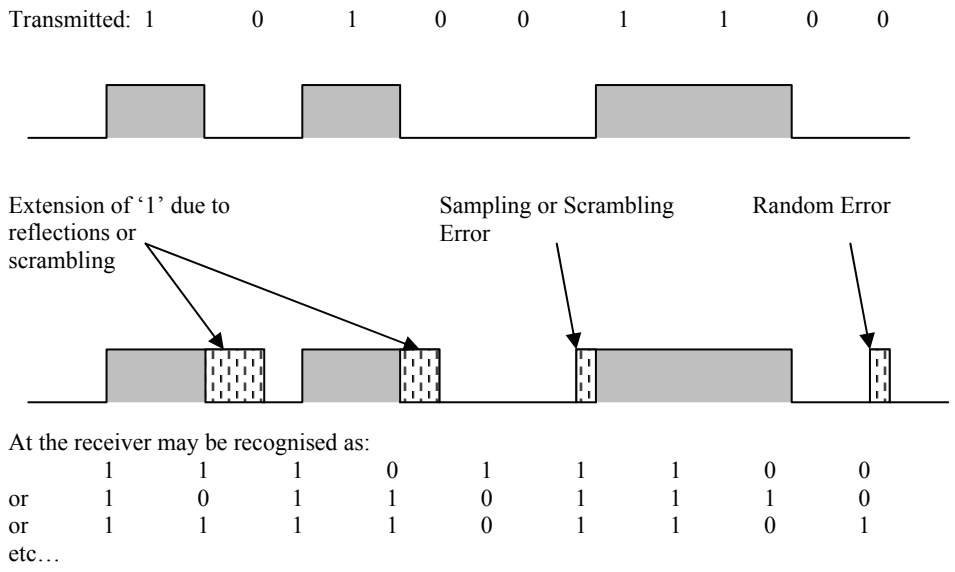

Fig. 8. Example errors during reception from the target

4. Decoding algorithms

The encoding of the signatures at the side of the transmitter is carried out through the well known Recursive Systematic Convolutional (RSC) encoder presented in Fig. 9 and described by the polynomial $(1+ D^2)/(1+D+D^2)$. If a signature is n-bits long, the encoded parity bits have also n-bits length. Each signature is interleaved and the interleaved signature bits are also encoded by the same RSC encoder. The n-bits of the original signature (SGN), its parity

bits that are generated by the RSC encoder (PA) and the parity bits of the interleaved signature (PB) are transmitted by the Sequencer module of the IRTX device as shown in Fig. 5b (code rate: 1/3). It is also possible that the interleaved signature is also transmitted in order to enhance the error correction capability at the side of the receiver by providing more redundant information (code rate: 1/4).

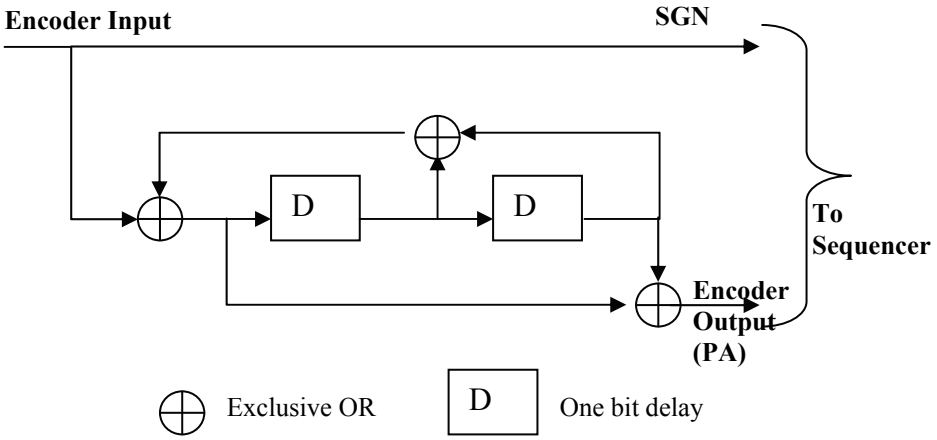

Fig. 9. Recursive Convolutional Encoder scheme employed

The encoding performed by the RSC state machine of Fig. 9 is also described by the state machine of Fig. 10 and the Trellis diagram of Fig. 11. The state names represent the output of the two Delay elements of the encoder. Each arrow in the state diagram is marked with the symbol *i/o,* where *i* is the input required for the state transition and *o* the resulting output of the RSC encoder.

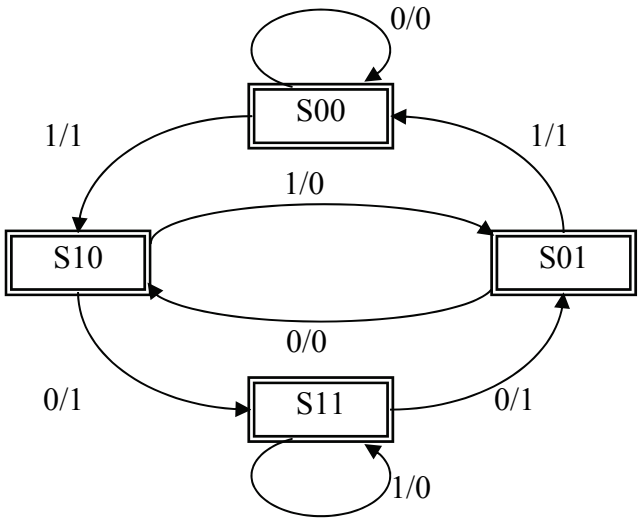

Fig. 9. The state diagram of the RSC encoder of Fig. 8

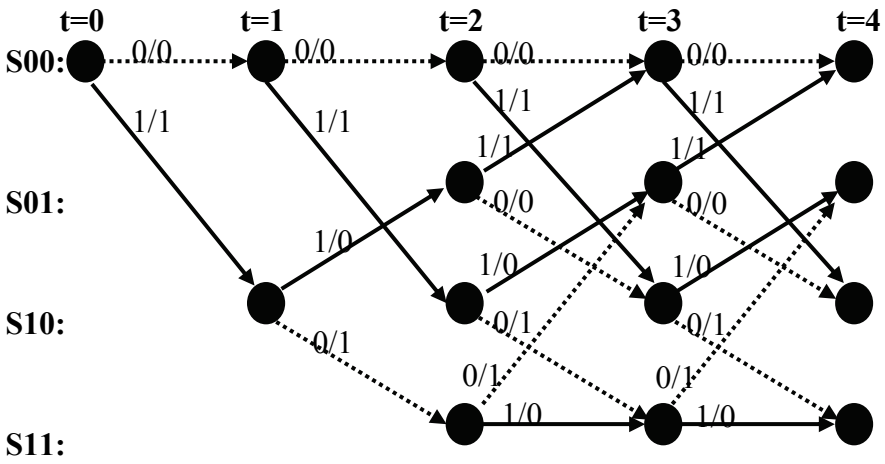

Fig. 10. The Trellis diagram of the RSC encoder of Fig. 8

The received signature and parity bits are input to the decoder. The decoder exploits the redundancy information of the parity bits in order to correct the error bits in the received signatures. The correction capability is strongly related to the SNR of the channel. If the SNR is too low, the decoder may not be able to correct all the error bits or it may even produce an output that has more error bits than its input. The decoder that we used is based on the Trellis diagram of Fig. 10. Every Trellis stage is implemented by the architectural blocks that are shown in Fig. 11.

The calculations performed at each one of the A-G blocks of Fig. 11 if a Sum-Product decoding algorithm is used (Hagenauer et al, 1996) are listed in Table 1. The input of each stage consists of: (a) the probabilities that $y_u(t)$ is received given that the transmitted data bit is 1 ($x_u(t)=1$) or 0 ($x_u(t)=0$), (b) the probabilities that $y_p(t)$ is received given that the transmitted parity bit is 1 ($x_p(t)=1$) or 0 ($x_p(t)=0$) respectively. Due to the conditional probabilities used as soft input, the decoder that is constructed by the blocks shown in Fig. 11 is called Soft In Soft Out decoder (SISO). In Turbo decoding, two SISO decoders need to be used in parallel as shown in Fig. 12 operating on either the interleaved or the uninterleaved received data. Each SISO decoder produces the extrinsic information (block F of Fig. 11) that is exploited by the complementary SISO decoder as intrinsic information (block B). The SISO decoders are activated in an iterative way i.e., SISO 1 uses the input and initial intrinsic information and produces extrinsic information that is interleaved and used along with the interleaved input by the SISO 2 decoder. The extrinsic information of SISO 2 is deinterleaved and provided as intrinsic info to SISO 1 that is activated next. This process is repeated for a specific number of iterations.

Blocks A and B of Fig. 11 estimate the branch metrics of the Trellis diagram from the data/parity input and the intrinsic information. Blocks C and D estimate the node metrics of the Trellis diagram which are propagating forwards (a_S) and backwards (b_S) through the Trellis. The blocks E, F and G combine the input, the node and the branch metrics in order to produce the output (block G) and the extrinsic information (block F).

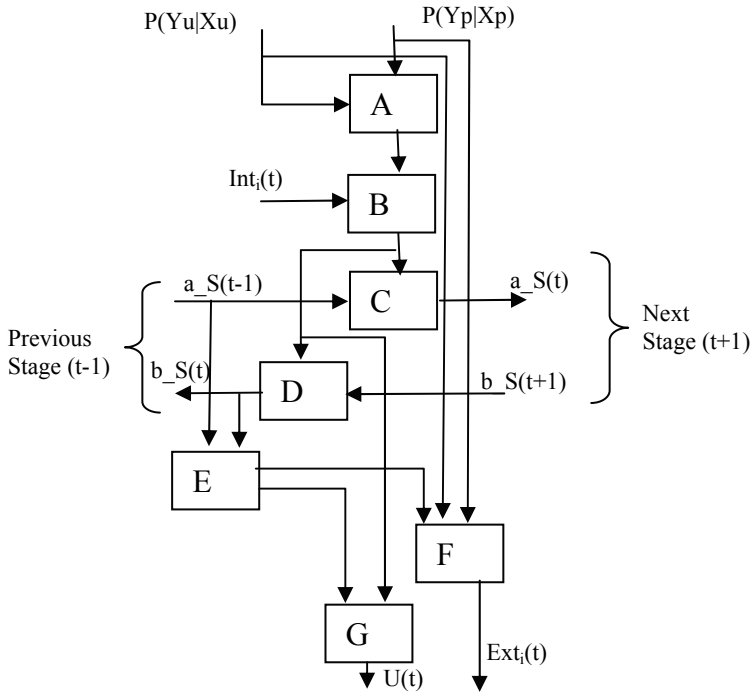

Fig. 11. Implementation of a Trellis decoder stage

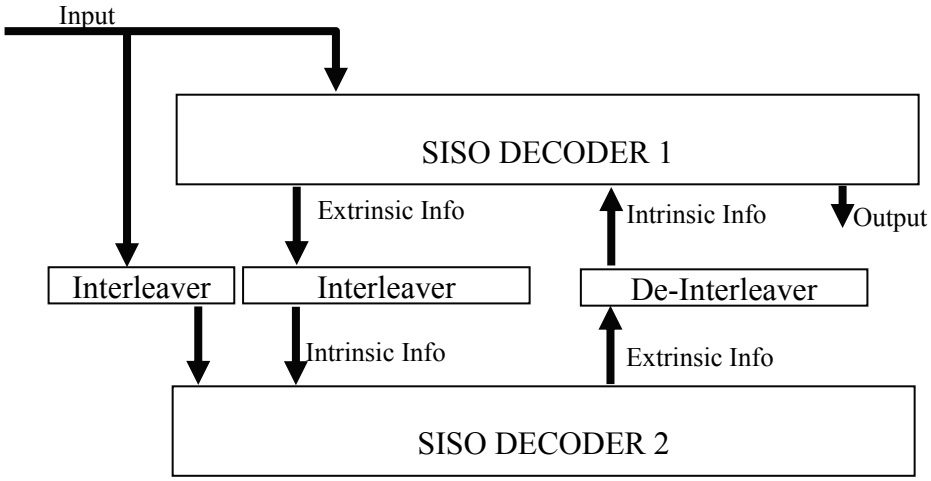

Fig. 12. A Turbo decoder

Block	Calculation
A	$\gamma'_{ij} = \Pr(y_u(t) \mid x_u(t) = i) \Pr(y_p(t) \mid x_p(t) = j)$, $i, j \in \{0,1\}$
B	$\gamma_{ij} = \gamma'_{ij} Int_i(t)$, $i, j \in \{0,1\}$
C	$a\_S(t) = \sum_{S'} a\_S'(t-1)\gamma_{S' \to S}$
D	$b\_S'(t) = \sum_{S} b\_S(t+1)\gamma_{S' \to S}$
E	$I_{ij} = \sum_{i/j, S' \to S} a\_S'(t-1) b\_S(t)$
F	$Ext_i(t) = \sum_j I_{ij} \Pr(y_p(t) \mid x_p(t) = j)$, $i \in \{0,1\}$
G	$U_i(t) = \sum_j I_{ij} \gamma_{ij}$, $i \in \{0,1\}$

Table 1. Calculations performed by the Sum-Product Algorithm

The operations listed in Table 1 are additions and multiplications. If the Sum-Product algorithm is implemented by the processing unit of the receiver of Fig. 2, then the processing unit should support multiplications of high accuracy. Lower cost processing units can be used if the Min-Sum or the Max-Log MAP algorithm is used instead of the Sum-Product. Specifically, by using the Andersen identity:

$$-\ln(e^{-x} + e^{-y}) = \min(x, y) - \ln(1 + e^{-|y-x|}) \tag{10}$$

and applying the –ln(x) function to the left and the right side of the expressions in the blocks A, B and C of Table 1 we get:

$$\begin{aligned} &\gamma'_{ij} = \Pr(y_u(t) \mid x_u(t) = i) \Pr(y_p(t) \mid x_p(t) = j) \Rightarrow \\ &-\ln(\gamma'_{ij}) = -\ln(\Pr(y_u(t) \mid x_u(t) = i)) - \ln(\Pr(y_p(t) \mid x_p(t) = j)) \Rightarrow \\ &\gamma''_{ij} = \Pr^{MS}(y_u(t) \mid x_u(t) = i) + \Pr^{MS}(y_p(t) \mid x_p(t) = j) \end{aligned} \tag{11}$$

$$\begin{aligned} &\gamma_{ij} = \gamma'_{ij} Int_i(t) \Rightarrow \\ &-\ln(\gamma_{ij}) = -\ln(\gamma'_{ij}) - \ln(Int_i(t)) \Rightarrow \\ &\gamma_{ij}^{MS} = \gamma''_{ij} + Int_i^{MS}(t) \end{aligned} \tag{12}$$

$$\begin{aligned} &a\_S(t) = \sum_{S'} a\_S'(t-1)\gamma_{S' \to S}(t) \Rightarrow \\ &-\ln(a\_S(t)) = -\ln(\sum_{S'} e^{-(-\ln(a\_S'(t-1)\gamma_{S' \to S}(t)))}) \Rightarrow \\ &a\_S^{MS}(t) = \min_{S'}(a\_S'(t-1) + \gamma_{S' \to S}(t)) + CorrectionFactor \end{aligned} \tag{13}$$

The correction factor appearing in (13) has the form of the second term at the right part of (10). If a similar transformation is applied to the rest of the blocks of Table 1 and the correction factor is omitted, then we get the expressions of the Min Sum Algorithm that are listed in Table 2.

Block	Calculation
A	$\gamma_{ij}^{"} = \Pr^{MS}(y_u(t) \mid x_u(t) = i) + \Pr^{MS}(y_p(t) \mid x_p(t) = j)$, $i, j \in \{0,1\}$
B	$\gamma_{ij}^{MS} = \gamma_{ij}^{"} + Int_i^{MS}(t)$, $i, j \in \{0,1\}$
C	$a\_S(t)^{MS} = \min_{S'}(a\_S'(t-1)^{MS} + \gamma_{S' \to S}^{MS})$
D	$b\_S'(t)^{MS} = \min_{S}(b\_S(t+1)^{MS} + \gamma_{S' \to S}^{MS})$
E	$I_{ij}^{MS} = \min_{i/j, S' \to S}(a\_S'(t-1)^{MS} + b\_S(t)^{MS})$
F	$Ext_i^{MS}(t) = \min_j(I_{ij}^{MS} + \Pr^{MS}(y_p(t) \mid x_p(t) = j))$, $i \in \{0,1\}$
G	$U_i^{MS}(t) = \min_j(I_{ij}^{MS} + \gamma_{ij}^{MS})$, $i \in \{0,1\}$

Table 2. Calculations performed by the Min-Sum algorithm

If (14) is used and ln(x) is applied instead of –ln(x) the expressions of the Max-Log MAP algorithm can be derived, but they are omitted since they are identical to the ones of Table 2 if *min* function is replaced with the *max* one.

$$\min(x, y) = -\max(-x, -y) \tag{14}$$

5. Simulation Results

The Sum-Product and the Min-Sum decoding algorithms described in the previous section have been simulated using as input the specific 160-bit signatures that are used in the localisation system of the present work and are listed in Table 3.

Non-equalised signatures		Equalised signatures	
IRTX1	IRTX2	IRTX1	IRTX2
0x01010101	0x66666666	0x88888484	0x89898c8c
0x11111111	0xaaaaaaaa	0x18181212	0x1c1c1313
0x15151515	0xa4a4a4a4	0xc8c8c4c4	0xc9c9cccc
0x55555555	0x44444444	0x38383232	0x3c3c3333
0x33333333	0x04040404	0xe3e3e7e7	0xe1e1f3f3

Table 3. The 160 bit signatures used

The non-equalised signatures consist of 5 parts where the frequency of the bit value 1 occurs is different in each one of these parts. Moreover, the transmission of 1's by IRTX1 is not overlapping with the transmission of 1's by IRTX2. Based on this fact, a lot of scrambling errors are expected during real time operation.
The definition of the equalised signatures is based on the use of signature parts by the two IRTX devices that differ in fewer bits than the non-equalised signatures in order to avoid scrambling. Moreover, the 1s are gathered together in order to reduce the errors caused by the reflections since less 1→0 transitions appear in the signatures as discussed in Section 3. The original signatures are transmitted along with the corresponding parity bits of the original and the interleaved signatures that are generated by the encoder. The techniques applied for reducing the scrambling and reflection errors in the equalised signatures do not have any effect in the parity bits since if for example less 1→0 transitions appear in the original signature, it is not guaranteed that fewer 1→0 transitions will also appear in the parity bits.
The only simulated noise is of AWGN type with the SNR being in the range of [-1dB..+2dB]. This SNR range has been experimentally determined by taking into consideration the total number of errors in the received patterns at various spots in the covered area.
Fig. 13 presents the simulated results for various Turbo iterations. The non-equalised signatures are tested with a Random Interleaver. The equalised signatures are tested with the same Random interleaver and with a 2-level interleaver as well that generates equalised interleaved signatures. The 2-level interleaver rotates to the right by 3 positions the 32-bit signature parts at the first level and then the internal 32-bits of each part are reversed. This type of interleaving is described in Fig. 14 for which the following expression holds:

$$Interleaver[32 \cdot i + j] = 32 \cdot ((i+3)\%5) + 31 - j \text{ ,} 0 \le i < 5,\ 0 \le j < 32 \tag{15}$$

Based on the diagrams of Fig. 13 it can be concluded that if the number of iterations is 10 or higher, the error correcting capability is not significantly improved. For this reason, the Turbo decoder at the position localisation system will use 10 iterations as the best trade off between decoder performance and speed.
The Min-Sum algorithm shows a 0.5dB penalty in its performance compared to the Sum-Product if the SNR is low due to the omission of the correction factor. If the SNR is high, these algorithms have the same performance. In our experimental setup the error correction algorithm is executed in the Host Computer. Hence, the Sum-Product algorithm is used in order to achieve a better error correcting performance.
The choice of a proper interleaver affects significantly the performance since the 2-level interleaver tested has 0.5dB penalty at low SNR and more than 1.5dB penalty if the SNR is higher than 1dB. Even if the interleaved signature is also transmitted (code rate 1/4), the final bit error rate of the corrected patterns will not be improved since although fewer errors will occur at the interleaved signature, the capability of correcting the rest of the errors is reduced. For this reason, for the position localisation system, the Random Interleaver is used with the equalised signatures that are transmitted along with the corresponding parity bits of the signatures (code rate 1/3).

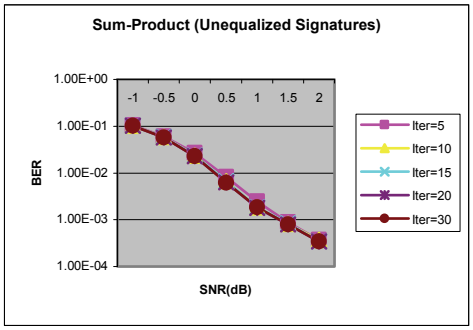

(a)

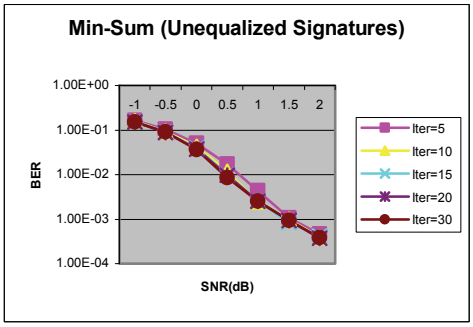

(b)

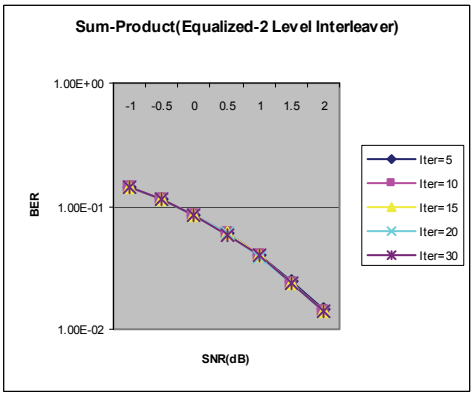

(c)

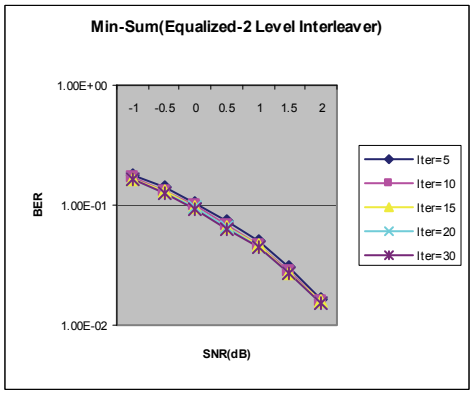

(d)

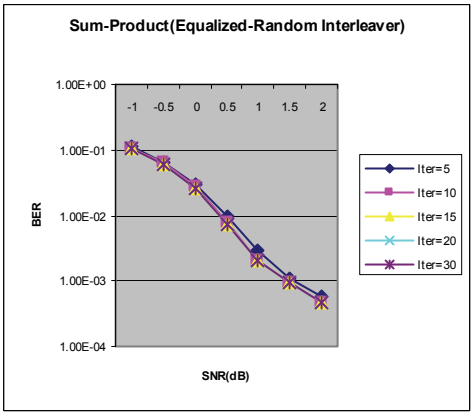

(e)

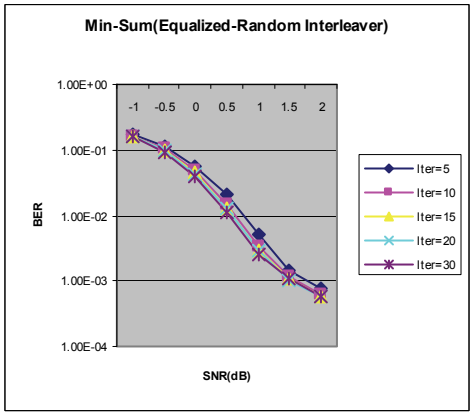

(f)

Fig. 13. Simulation results for the Sum-Product and the Min-Sum algorithms

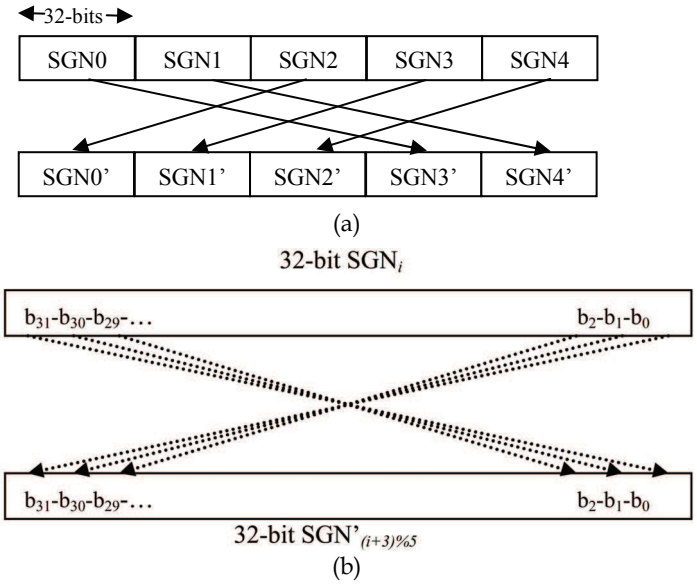

Fig. 14. A 2-level interleaver that generates equalised signatures

6. Experimental setup

The experimental setup beyond the signatures listed in Table 3 include also a number of short 8-bit signatures. The latter were not simulated in the previous section due to the fact that it is known that Turbo decoding has not considerable effect on data blocks with short length. We define the following signature structures that were experimentally tested:

6.1 Previous architecture (Setup1)

This is the previous setup described in (Petrellis et al, 2007). The patterns transmitted have the form of Fig. 4. The IRTX1 device transmits MOD2, MOD5, MOD6, MOD9 while IRTX2 transmits MOD3, MOD4, MOD7 and MOD8. The IRTX devices are independent and transmit concurrently. The number of the received pattern codes of each type is used as a multidimensional position identity. The time needed to transmit all the supported patterns between two preambles is:

$$T_{setup1} \propto 10\max(2T_2 + 5T_5 + 6T_6 + 9T_9, \\ 3T_3 + 4T_4 + 7T_7 + 8T_8) \tag{16}$$

The parameter T_i is the duration of a pulse in MOD*i*. If the time needed to transmit a bit in the rest of the setups is T_b, then the following values have been chosen for T_2-T_9: T_9=T_b, T_9<T_8<…< T_2. The pause interval between the successive patterns transmitted is $10T_b$.

6.2 Overlapping 8-bit signatures (Setup2)

The new architecture with a Sum-Product Turbo Decoder is used. Five short 8-bit signatures are transmitted along with their corresponding randomly interleaved signatures and their

parity bits (code rate 1/4). The receiver tests alternatively the original or the interleaved signature bits as input to the decoder and uses the best results that are obtained. The two IRTX devices are independent and transmit concurrently. The set of signatures that are transmitted by IRTX1 is {0x85, 0x94, 0xa9, 0xd5, 0xbb} while IRTX2 transmits: {0x24, 0x4c, 0x5a, 0x3b, 0x6f}. These signatures have been selected so that each one of them differs in the number 1's. This is expected to force the receiver to recognise each one of these signatures with different error rate and hence, a multidimensional identity will be assigned to the specific position of the target. If s is the number of signatures, r is the code rate and b the number of bits per signature, then the time needed to transmit a set of signatures is:

$$T_{setup2} \propto \frac{s \cdot b \cdot T_b}{r} \tag{17}$$

6.3 Non-overlapping 8-bit signatures (Setup3)

Similar to Setup2 but the IRTX devices transmit in a non overlapping manner i.e., the IRTX1 does not transmit when IRTX2 does and vice versa. The signatures in this setup are received from the channel with lower bit error rate since scrambling is avoided. The time needed to transmit a set of signatures in this case is:

$$T_{setup3} \propto 2\frac{s \cdot b \cdot T_b}{r} \tag{18}$$

6.4 Overlapping 160-bit signatures (Setup4)

The non-equalised signatures of Table 3 are transmitted concurrently by the two IRTX devices. The interleaved signature bits are not transmitted (code rate 1/3). The time needed to transmit the signature and the parity bits is determined by (17).

6.5 160-bit signatures. One IRTX transmitting (Setup5)

Similar to the Setup4 but only one IRTX device is transmitting. The position identities are formed by 5 signature match degrees instead of 10 since the single IRTX device transmits a 160-bit signature with 5 parts. This setup is tested in order to see whether a second IRTX device is really necessary. The time needed to transmit the signature and the parity bits is determined again by (17).

6.6 Non-Overlapping 160-bit signatures (Setup6)

Similar to the Setup4 but the IRTX devices transmit in a non overlapping manner in order to avoid scrambling. The time needed to transmit the signature and the parity bits is determined by (18).

6.7 Equalised 160-bit signatures (Setup7)

The equalised signatures of Table 3 are used in order to let the IRTX devices transmit concurrently but achieve a lower bit error rate at the channel due to the structure of the signatures. The code rate is again 1/3 since the interleaved signatures are not transmitted. The time needed to transmit the signature and the parity bits is determined by (17).

7. Experimental results - discussion

The experiments for each of the aforementioned set-ups (described in the previous section) were performed with the IRTX1 and IRTX2 placed in 2.5m vertical distance and 60cm horizontal displacement as shown in Fig. 1. We focused in a region of 2.5mx1.5m between the two IRTX devices where the signal of both transmitters is strong. A virtual grid with 30cmx30cm squares is assumed to cover this region. The coordinates of a grid node or a real target position within this region are represented as (y,xD), where y is the vertical distance from IRTX1, x the horizontal displacement from IRTX1 and D denotes whether the target is on the Left (L) or the Right (R) of the IRTX1 device.

During the calibration stage that was carried out in each setup before real time operation, the target visited the nodes of the grid and stored the measured signature (parts) matching degrees. Then, during real time operation the target visited positions that were closer to each one of the grid nodes listed in Table 4. In each one of these positions, 5 localisation procedures were carried out repeatedly. The results of these localisation procedures are not all identical. If at least one of them finds the closer grid node or one of the other three neighbouring grid nodes, the position is marked as Successful (S), or Acceptable (A) respectively, otherwise it is marked as Fail (F). The exact results for each position are presented in Table 4.

In the first column the position coordinates are listed and the mark of the position appears in column C1. If a position is marked as Successful, the column C2 has a number that indicates how many of the 5 localisation procedures led to the closer grid node while column C3 indicates how many localisation procedures led to an acceptable grid node. Column C4 shows how many different grid nodes were selected in each position by the localisation procedures. The asterisk in Setup3-Setup7 marks a position in which the Turbo Decoding results were used. We do not have such an indication in Setup2 although Turbo Decoding was used in that case too, since in this setup the better results of Turbo Decoding on either the interleaved or the original signatures are always used.

Position	Setup 1				Setup 2				Setup 3				Setup 4				Setup 5				Setup 6				Setup 7			
	C1	C2	C3	C4	C1	C2	C3	C4	C1	C2	C3	C4	C1	C2	C3	C4	C1	C2	C3	C4	C1	C2	C3	C4	C1	C2	C3	C4
30,30L	A		2	2	F			1	F*			1	F			1	A*		3	2	A*		2	3	S	1	2	2
30,30R	S	2		2	A		2	2	F*			1	S	2	1	5	S*	1		1	S*	1	2	3	A		2	4
60,30L	S	3		2	A		5	2	F*			1	A*		2	2	A*		2	3	F*			1	F*			1
60,0	S	2	2	3	A		3	1	F*			1	F			1	S	2	2	4	A*		3	3	A		3	2
60,30R	A		2	2	S	5		1	F			1	A*		1	3	A*		2	5	S*	2	2	3	S	1	3	3
60,60R	S	1	3	3	F			2	A		5	1	A		2	5	F			1	F			3	S	2	1	4
90,60L	F			2	S	5		1	F			1	S*	5		1	F*			2	S*	5		1	A*		3	3
90,0	F			2	A		5	1	F			1	A		3	3	A		5	2	S	2		2	F			1
90,30R	F			2	S	5		1	F			1	S	1		4	A		5	3	A		2	3	S*	2	1	3
90,60R	S	2	1	4	A		5	1	F*			1	F			2	F			3	F			2	A		5	4
120,30L	F			4	F			5	F			1	A*		5	1	A*		3	4	A*		5	1	S	1	2	3
120,30R	F			3	A		4	2	F*			1	S	2	3	2	S	3		3	S	2	2	4	A		1	3
150,0	A		1	5	F			1	F			1	A		4	3	A		5	1	S	3		2	S	1	4	3
150,60R	F			1	S	5		1	A*		3	3	A		5	4	A*		1	3	S	2	2	4	S	3		1
180,30L	A		1	2	F			1	F			1	F			2	F*			2	A*		3	3	F			1
180,0	S	1	4	2	A		5	1	A		5	1	A		3	3	F			2	S	3	2	2	A		2	2
180,30R	A		4	2	S	3	2	2	A*		5	1	A		5	2	A		2	2	S	3	2	3	S*	1	2	4
210,0	S	4		2	S	5		1	A*		5	1	S	2		3	F*			3	S	5		1	F			1
210,60R	S	5		1	S	1		3	S*	1	4	2	S*	1	2	2	F*			1	A*		4	3	S	3		2
Totals	8S 5A 6F	20	20		7S 7A 5F	29	33		1S 5A 13F	1	27		6S 9A 3F	13	36		3S 9A 7F	6	30		10S 6A 3F	30	31		9S 6A 4F	17	31	

Table 4. The experiment results

Based on the results of Table 4 the accuracy and stability results can be obtained for each setup. Achieving a successful estimation is 3 times more important than an acceptable estimation since for a specific position there is only one successful node and three acceptable nodes among the ones of the whole grid. Using this fact the accuracy and stability results are

compared in Fig. 15a and Fig. 15b. The speed of a localisation procedure in each setup is determined by the delay estimated by the expressions: (16)-(18). These expressions lead to the speed comparison of Fig. 15c.

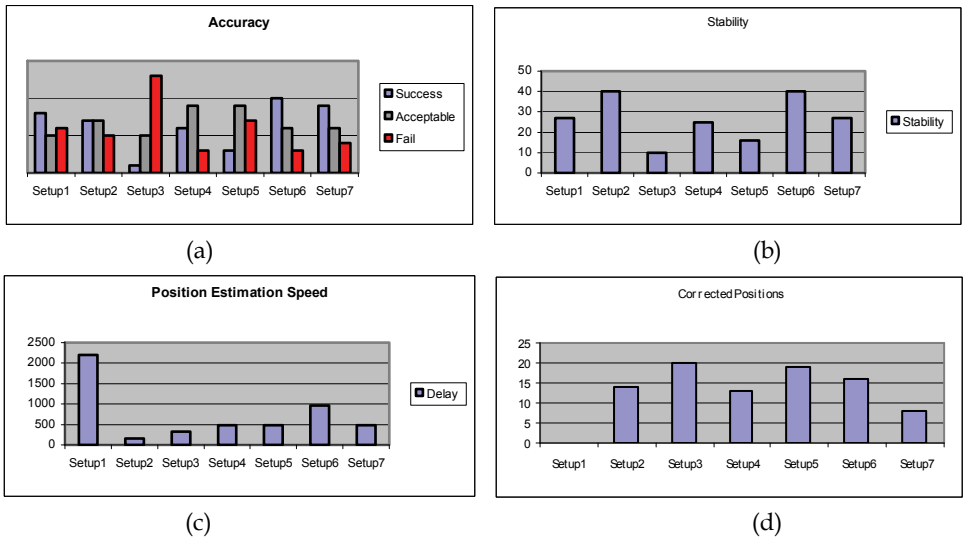

Fig. 15. Setup Comparison

Fig. 15d, presents the number of nodes where Turbo Decoding of the original signatures was exploited during the calibration stage, since error correction was achieved. Error correction could not be achieved in the rest positions due to the fact that the SNR is extremely low there.

The results with the best accuracy are obtained by Setup6 followed by Setup7 where non-overlapping or equalised signatures are used respectively. Nevertheless, Setup7 is twice as fast as Setup6. Setup2 is the fastest and the most stable setup, but produces results with moderate accuracy. This is due to the fact that short signatures are received with a small number of errors. Most of these few errors are further corrected by the Turbo Decoder. This leads to position identities that do not differ enough and may be easily confused with each other. This impact of this fact is worse in Setup3 where the signatures are transmitted in a non overlapping manner. Setup3 is twice slower than Setup2 and produces the worse accuracy results.

Besides the wider area coverage, the use of a second IRTX device improves the accuracy and the stability results of a localisation procedure since these features are not quite good in Setup5 where a single IRTX device was used.

Concluding, it can be said that all the new setup architectures tested are 2-13 times faster than our previous setup and most of them provide better accuracy and stability results. The use of equalised signatures in Setup7 seems to provide the best trade off between speed accuracy and stability.

8. Conclusions

Several new position estimation methods based on the error rate of received infrared patters were discussed in this chapter. The estimation of the features of the infrared channel of the

positioning system allowed the selection of appropriate pattern structures and forward error correction methods that improve the speed, the accuracy and the stability of the localisation procedure. This is due to the fact that the impact of instant noise that cannot be taken into consideration during the calibration stage was limited.
Future work will focus on testing other pattern types as well as different forward correction techniques like Viterbi or LDPC. Moreover, different encoders with more delay elements will also be tested in order to correct more efficiently shorter patterns.

9. References

Arzel, M. Lahuec, C., Seguin, F., Gnaedig, D. & Jezequel, M. Semi-Iterative Analog Turbo Decoding. *IEEE Transactions on Circuits and Systems*. Vol. 54, No. 6, 2007, pp. 1305-1315

Arras, K., Tomatis, N., Jensen, B. & Siegward, R., Multisensor On-the-Fly Localisation : Precision and Reliability for Applications. *Elsevier Robotics and Autonomous Systems*, 43(2001), pp. 131-143.

Aytac, T. & Barshan, B., Simultaneous Extraction of Geometry and Surface Properties of Targets Using Simple Infrared Sensors. *Optical Engineering,* 43(10), Oct. 2004, pp. 2437-2447

Baskent, D. & Barshan, B. Surface Profile Determination from Multiple Sonar Data Using Morphological Processing. *Int. Journal of Robotics Research*. Vol .18, No. 8, 1999, pp. 788-808

Benet, G, Blanes, F., Simo, J. & Perez, P. Using Infrared Sensors for Distance Measurement in Mobile Robots. *Robot Autonomy Systems,* Vol. 30, 2002, pp. 255-266

Bicho, E., Mallet, P. & Schoner, G. Target Representation on an Autonomous Vehicle with Low Level Sensors, *Int. Journal of Robotics Research,* Vol. 19, No. 5, May 2000, pp. 424-447

Bickerstaff M.A., Garret D., Prokop T., Thomas C., Nicol C., A 24 Mb/s radix-4 logMAP Turbo decoder for 3GPP-HSDPA mobile wireless, *in Proc. IEEE Int. Solid-State Circuits Conf., San Francisco, pp.150-151, Feb. 2003.*

Borenstein, J. Everett, B. & Feng, L. (1996). *Navigating Mobile Robots: Systems and Techniques*, A.K. Peters Ltd Wellesley, MA

Clerentin A., Delahoche, A., Brassart, E. & Drocourt, C. Self Localisation: A New Uncertainty Propagation Architecture. *Elsevier Robotics and Autonomous Systems*, 51(2001), pp. 151-166

Flora, C., Ficco, M., Russo, S. & Vecchio, V. Indoor and Outdoor Location Based Services for Portable Wireless Devices. *Proceedings of 1st IEEE Int. Workshop on Services and Infrastructure for Ubiquitous and Mobile Internet,* pp. 244-250, June 2005, Columbus OH

Gamal, H. & Hammons, R. Analyzing the Turbo Decoder Using Gaussian Approximation. *IEEE Transactions on Information Theory*. Vol. 47, No. 2, 2001, pp. 671-686

Gioulekas, F., Birbas, M., Birbas, A., Bilionis, G: Analog Error-Correcting Decoders Using SiGe BiCMOS Technology. *International Journal of Analog Integrated Circuits and Signal Processing, Springer,* Vol. 52, No. 3 pp.117-132. October 16, 2007

Hagenauer, J. Offer, E. & Papke, L. Iterative Decoding of Binary Block and Convolutional Codes. *IEEE Transactions on Information Theory*. Vol. 42, No. 6, 1996, pp. 429-445

Jin, T., Lee, J. & Tso, S. A New Space and Time Sensor Fusion Method for Mobile Robot Navigation. *Wiley Journal of Robotics Systems*, 21(7), 2004, pp. 389-400

Kosel, J. Pfutzner, H., Mehnen, L., Kaniusas, E., Meydan, T., Vazquez, N., Rohn, M., Merlo, A. & Marquardt, B. Non Contact Detection of Magnetoelastic Position Sensors. *Elsevier Sensors and Actuators A*, 123-124 (2005), pp. 349-353

Kschischang, F., Frey, B. & Loeliger, H. Factor Graphs and the Sum-Product Algorithm. *IEEE Transactions on Information Theory*. Vol. 47, No. 2, 2001, pp. 498-519

Ladd, A., Bekiris, K., Rudys, A., Kavraki, L. & Wallach, D. Robotics Based Location Sensing Using Wireless Ethernet. *Wireless Networks,* Vol. 11, No. 1-2, Jan 2005, pp. 189-204

Minami, M., Fukuju, Y., Hirasawa, K., Yokoyama, S., Mizumachi, M., Morikawa, H. & Aoyama, T. Dolphin: A Practical Approach for Implementing a Fully Distributed Indoor Ultrasonic Positioning System. *Lect Not Comp Sci,* 3205, 2004, pp. 347-365

Miura, J., Negishi, Y. & Shirai, Y. Adaptive Robot Speed Control by Considering Map and Motion Uncertainty. *Elsevier Robotics and Autonomous Systems,* 54(2006), pp. 110-117

Novotny, P. & Ferrier, N. Using Infrared Sensors and the Phong Illumination Model to Measure Distances. *Proceedings of the IEEE Int. Conf. On Robotics and Automation,* pp. 1644-1649, 1999, Detroit MI

Petrellis, N. Konofaos, N. & Alexiou, G. A Sensors System for Indoor Localisation of A Moving Target Based on Infrared Pattern Recognition. *I-Tech Scene Reconstruction, Pose Estimation and Tracking*, Chapter 16 (2007), pp. 283-304

Petrellis, N. Konofaos, N. & Alexiou, G. Using Future Position Restriction Rules for Stabilizing the Results of a Noise-Sensitive Indoor Localization System. *Optical Engineering*, 46(6), 2007, pp. 067202-1-067202-11

Prigge, E. & How, J. Signal Architecture for Distributed Magnetic Local Positioning System. *IEEE Sensors Journal.* Vol. 4, No. 6, 2004, pp. 864-873

Schlageter, V., Besse, P., Popovic, R. & Kucera, P. Tracking System with 5deg of Freedom Using a 2D Array of Hall Sensors and a Permanent Magnet. *Elsevier Sensors and Actuators A,* 92, 2001, pp. 37-42

Schlegel, C. & Perez, L. Trellis and Turbo Coding, *IEEE Series on Digital & Mobile Communication*, Wiley Interscience (2004)

Se, S., Lowe, D. & Little, J. Mobile Robot Localisation and Mapping With Uncertainty Using Scale Invariant Visual Landmarks. *Int. Journal of Robotics Research.* Vol. 21, No. 8, 2002, pp. 735-758

Smith, P. & Zografos, K. Sonar for Recognizing the Texture of Pathways. *Robotics and Autonomous Systems.* Vol. 51, 2005, pp. 17-28

Tardos, J., Neira, J., Newmann, P. & Leonard, J. Robust Mapping and Localization In Indoor Environments Using Sonar Data. *Int joural of Robotics Research.* Vol 21, No. 8, 2002, pp. 311-330

Tovar, B., Gomez, L., Cid, R., Miranda, M., Monroy, R. & Hutchinson, S. Planning Exploration Strategies for Simultaneous Localisation and Mapping. *Elsevier Robotics and Autonomous Systems.* 54(2006), pp. 314-331

Vasic, B. & Kurtas, E. (2005) *Coding and Signal Processing for Magnetic Recording Systems*. CRC Press, NY

Victorino A., Rives, P. & Borelly, J. Safe Navigation for Indoor Mobile Robots Part II: Exploration, Self Localisation and Map Building. *Int. Journal of Robotics Research*. Vol. 22, No. 12, Dec 2003, pp. 1019-1039

Pattern Recognition Techniques, Technology and Applications

Edited by Peng-Yeng Yin

ISBN 978-953-7619-24-4
Hard cover, 626 pages
Publisher InTech
Published online 01, November, 2008
Published in print edition November, 2008

A wealth of advanced pattern recognition algorithms are emerging from the interdiscipline between technologies of effective visual features and the human-brain cognition process. Effective visual features are made possible through the rapid developments in appropriate sensor equipments, novel filter designs, and viable information processing architectures. While the understanding of human-brain cognition process broadens the way in which the computer can perform pattern recognition tasks. The present book is intended to collect representative researches around the globe focusing on low-level vision, filter design, features and image descriptors, data mining and analysis, and biologically inspired algorithms. The 27 chapters coved in this book disclose recent advances and new ideas in promoting the techniques, technology and applications of pattern recognition.

InTech Europe
University Campus STeP Ri
Slavka Krautzeka 83/A
51000 Rijeka, Croatia
Phone: +385 (51) 770 447
Fax: +385 (51) 686 166
www.intechopen.com

InTech China
Unit 405, Office Block, Hotel Equatorial Shanghai
No.65, Yan An Road (West), Shanghai, 200040, China
中国上海市延安西路65号上海国际贵都大饭店办公楼405单元
Phone: +86-21-62489820
Fax: +86-21-62489821